ISSN 1068-7998, Russian Aeronautics, 2019, Vol. 62, No. 4, pp. 651–660. © Allerton Press, Inc., 2019.
Russian Text © The Author(s), 2019, published in Izvestiya Vysshikh Uchebnykh Zavedenii, Aviatsionnaya Tekhnika, 2019, No. 4, pp. 115–123.

AIRCRAFT AND ROCKET ENGINE DESIGN AND DEVELOPMENT

Micro Gas Turbine Engine for Unmanned Aerial Vehicles

V. A. Sychenkov[a], A. S. Limanskii[a], W. M. Yousef[a], V. V. Ankudimov[a, *], and S. S. Seyid Jafari[a]

[a]*Tupolev Kazan National Research Technical University, ul. Karla Marksa 10, Kazan, 420111 Tatarstan, Russia*

**e-mail: vladimir.ankudimov@inbox.ru*

Received July 19, 2019; in final form, October 28, 2019

Abstract—The results of development and manufacture of a micro gas turbine engine for an unmanned aerial vehicle are presented. The calculation features of the main elements of the engine blading section, namely, a centrifugal compressor, a reverse-flow combustor, and a radial-axial turbine are considered. The design of the inlet and output duct, rotor bearings, and lubrication system is described.

DOI: 10.3103/S1068799819040160

Keywords: micro gas turbine engine, unmanned aerial vehicle, turbocharger, centrifugal compressor, reverse-flow combustor, radial-axial turbine.

Design and attempts to manufacture micro gas turbine engines (MGTE) that started in the 1960s, resulted in the first works in this line [1, 2]. The subsequent works [3, 4] generated wide attention and increased the concern in the MGTE development. Recently, a number of papers have been published [5–11] that describe current approaches to the design of MGTEs using numerical methods for modeling processes and new technologies. Nevertheless, there is the lack of papers describing the practical application of the MGTE design technique.

This paper discusses the development and manufacture of a low thrust engine (up to 100 N). Due to the fact that the scaling principle of large-sized gas turbine engines cannot be applied during its design, a calculation technique was developed that takes into account the small size of its main components, flow regimes (Reynolds numbers, hydraulic loss coefficients in the engine paths, etc.) and their influence on the efficiency of parts. In [12], the authors consider the problem of selecting a structural design, the compressor and turbine model, a combustor scheme, the design of bearing joints, etc.

Figure 1 shows a CAD model of the MGTE created in the KOMPAS 3D software.

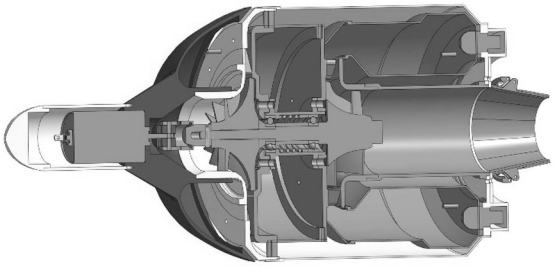

Fig. 1.

The MGTE inlet consists of a head fairing, in which the electric starter is located, and an air intake made by the additive polylactide technology (providing the reduced structural weight) and having a layout close to the lemniscate.

DEVELOPMENT OF A TURBOCHARGER

Taking into account that the creation of a novel MGTE requires certain design, production and technological expenditures, the development of its turbocharger was carried out on the basis of the existing TKR-7S-6 prototype that is used to pressurize the internal combustion engine of the KamAZ-740 automobile. The initial turbocharger consists of a centrifugal compressor, a radial-axial turbine connected by a common shaft, where swing bearings are used as sliding bearings (they are lubricated from the internal combustion engine lubrication system). A vaneless diffuser is located behind the impeller of the centrifugal compressor and a snail-shaped nozzle assembly is arranged in front of the impeller of the radial-axial turbine.

In order to reduce the dimensions of the turbocharger, the prototype underwent the following modification: the vaneless diffuser of the centrifugal compressor was replaced by a vaned diffuser [13], and its blades were made rectilinear with a wedge angle $\gamma = 8$ deg, with rounded inlet and outlet edges (Fig. 2). The following radial dimensions were selected: $D_3 = 0.084$ m, $D_4 = 0.14$ m, the blade height $h_d = 5.1$ mm; curvature profile: $r_3 = 0.5$ mm, $r_4 = 1$ mm, $R_4 = 5$ mm.

In shaping the vaned diffuser (Fig. 3), the number of blades was selected to get the angle of diffuser (the diffuser inlet) no more than $\theta_d = 8 - 9$ deg, which ensures an uninterrupted flow in the blade passage, and the number of blades is determined by the dependence [14]:

$$z_d = \frac{\pi D_4 \sin\alpha_{4b} D_3 \sin\alpha_{3b}}{2 b_d \theta_d}, \tag{1}$$

where the blade angle at the inlet to the vaned diffuser $\alpha_{3b} = 27$ deg was determined from the velocity triangle at the exit of the impeller of the centrifugal compressor, the blade angle at the exit is determined as

$$\alpha_{4b} = \arccos\left(\cos\alpha_{3b}\frac{D_3}{D_4}\right). \tag{2}$$

In the calculations we have $\alpha_{4b} = 57.7$ deg.

The blade chord is determined by the following relation:

$$b_d = \frac{D_4 \sin(\alpha_{4b} - \alpha_{3b})}{2\cos\alpha_{3b}}. \tag{3}$$

In the calculations $b_d = 31.5$ mm. The number of blades obtained is $z_d = 20$.

Fig. 2.

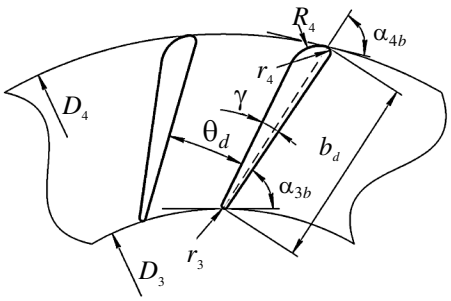

Fig. 3.

In thermogasdynamic calculation of the flow section of the centrifugal compressor [15], the following inlet data were selected: the air flowrate as in the prototype $G_a = 0.275$ kg/s, the optimum rotor speed for

a turbocharger $n=84000\ \text{min}^{-1}$, the gas temperature in front of the radial-axial turbine $T_g = 1100\ \text{K}$. In this case, the optimal pressure coefficient of the centrifugal compressor was taken

$$\bar{H}_{cS} = \frac{H_{cS}}{u_c^2} = 0.56, \tag{4}$$

whence the isentropic pressure $H_{cS} = 62846\ \text{J/kg}$ [13], at a peripheral speed of the outer diameter of the impeller $u_c = 335\ \text{m/s}$.

The compressor pressure ratio is

$$\pi_c^* = \left(\frac{H_{cS}}{\frac{k}{k-1} R_a T_{atm}} + 1 \right)^{\frac{k}{k-1}}, \tag{5}$$

where $k = 1.4$; $R_a = 287 \frac{\text{J}}{\text{kg} \cdot \text{K}}$; $T_{atm} = 288\ \text{K}$. In calculations $\pi_c^* = 2$.

The compressor outlet pressure is

$$P_c^* = \pi_c^* P_{atm}^* \sigma_{in}^*, \tag{6}$$

where the standard atmospheric pressure is $P_{atm}^* = 101325\ \text{Pa}$, the input pressure recovery coefficient $\sigma_{in}^* = 0.98$. In calculations $P_c^* = 1.986 \times 10^5\ \text{Pa}$.

The compressor outlet temperature is

$$T_c^* = T_{atm}^* \pi_c^{* \frac{k-1}{k \eta_{st}}}, \tag{7}$$

where the polytropic stage efficiency is $\eta_{st} = 0.75$. In calculations $T_c^* = 375\ \text{K}$.

According to the results of calculating the pressure loss, the pressure recovery coefficient in the vaned diffuser of the centrifugal compressor was $\sigma_d^* = 0.985$. In the outer annular path, taking into account the axial flow rotation, $\sigma_{tr}^* = 0.98$, in the combustor $\sigma_{comb}^* = 0.95$. Therefore, the pressure at the inlet to the nozzle apparatus of the radial-axial turbine is determined as

$$P_{g0}^* = P_c^* \sigma_\Sigma, \tag{8}$$

where the total pressure recovery coefficient in the nodes listed is

$$\sigma_\Sigma = \sigma_d^* \sigma_{tr}^* \sigma_{comb}^* = 0.92. \tag{9}$$

In calculations $P_{g0}^* = 1.827 \times 10^5\ \text{Pa}$.

A vaned nozzle apparatus was used in the radial-axial turbine instead of a snail-shaped nozzle apparatus as in the prototype. To simplify the design, we selected the type of shaping the nozzle blades of simple shape with rectilinear parallel generators, the so-called wing-shaped blades, the profile of which has a relatively thickened profiled outer edge (Fig. 4) [15]. In the design calculation of the nozzle blades of the radial-axial turbine, the following basic geometric dimensions of the prototype were taken: the outer diameter of the nozzle apparatus $D_0 = 0.102\ \text{m}$; the diameter at the exit of nozzle blades $D_{1nb} = 0.078\ \text{m}$; the impeller outer diameter $D_{1im} = 0.0735\ \text{m}$; the outer diameter at the exit of the impeller $D_{2im} = 0.0643\ \text{m}$; the impeller hub diameter $D_{imh} = 0.0225\ \text{m}$; the nozzle blade height $h_{1nb} = 0.0096\ \text{m}$.

Shaping of the nozzle apparatus (Fig. 5) was carried out with the number of blades $z_{nb} = 20$. A larger number suggests a reduced size of the "throat", namely, the narrowest point of the channel, which causes technological difficulties during machining.

Fig. 4.

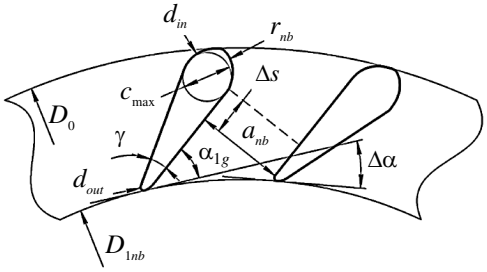

Fig. 5.

With a given number of blades, their wedge angle, deg, is

$$\gamma = \frac{360}{z_{nb}} = 18\,. \tag{10}$$

The optimal parameter of the radial-axial turbine was chosen [11]:

$$\left(\frac{u_{1im}}{c_{tS}}\right)_{opt} = 0.67\,, \tag{11}$$

where $u_{1im} = 323.1$ m/s is the peripheral velocity of the peripheral part of the impeller. Hence, the isentropic velocity is $c_{tS} = 482.24$ m/s.

Then the available heat drop of the radial-axial turbine is determined [16]:

$$L_{tS} = \frac{c_{tS}^{\,2}}{2}\,. \tag{12}$$

In the calculations $L_{tS} = 11628$ kJ/kg..

In choosing the degree of reaction of the turbine stage ρ_t, the condition [17] was fulfilled:

$$\rho_t > \rho_{t\,\min}\,,$$

where the minimum reactivity is

$$\rho_{t\,\min} = \left(\frac{u_{1im}}{c_{tS}}\right)^2 \left(1 - \mu_{av}^{\,2}\right) = 0.293\,. \tag{13}$$

Here the radial coefficient is $\mu_{av} = \dfrac{D_{2av}}{D_{1im}} = 0.59$, where the average diameter at the impeller exit is $D_{2av} = \dfrac{D_{2im} + D_{im.h}}{2} = 0.0434$; the optimal degree of reaction is $\rho_t = 0.38$.

The isoentropic work of gas expansion in a nozzle blade is:

$$L_{nbS} = L_{tS}\left(1 - \rho_t\right). \tag{14}$$

In calculations $L_{nbS} = 72.09$ kJ/kg.

The speed at the exit of the nozzle blade is

$$c_1 = \varphi_{nb}\sqrt{2L_{nbS}}\,, \tag{15}$$

where $\varphi_{nb} = 0.92$ is the nozzle blade speed coefficient; in calculations $c_1 = 349.3$ m/s.

In constructing the profile of a radial nozzle blades, in comparison with the axial ones, there is a special feature, namely, the effective angle α_{1e}, which for the known gas flowrate and the height of the blades is determined from the flowrate equation

$$\alpha_{1e} = \arcsin\frac{G_g}{\pi D_{1nb}\rho_1 c_1 h_{1nb}}, \tag{16}$$

where the gas density at the exit of the nozzle apparatus is $\rho_1 = 0.511$ kg/m^3. We get the angle $\alpha_{1e} = 38.4$ deg in calculations.

The geometric angle at the exit of the nozzle apparatus is related to the effective angle α_{1e} by the ratio

$$\alpha_{1g} = \alpha_{1e} - \Delta\alpha\,. \tag{17}$$

Here the additional rotation α_{1e} in comparison with the geometric angle α_{1g} by $\Delta\alpha$ is due to the feature of the radial flow and is half the angle between the blades:

$$\Delta\alpha = \frac{\gamma}{2} = 9\,. \tag{18}$$

Thus, $\alpha_{1g} = 29.4$ deg.

The dependence of the "throat" a_{nb} on the effective angle is written as follows:

$$a_{nb} = \frac{t_{1nb}\sin\alpha_{1e}}{k_{nb}} - d_{out}\,. \tag{19}$$

Here the experimental coefficient is $k_{nb} = 1.05$ [17], the outlet edge diameter is $d_{out} = 0.4$ mm; in calculations $a_{nb} = 6.8$ mm.

The nozzle blade pitch taken along the chord t_{1nb} can be replaced by the step calculated along the arc t'_{1nb}:

$$t_{1nb} \cong t'_{1nb};\ t'_{1nb} = \frac{\pi D_{1nb}}{z_{nb}}\,. \tag{20}$$

Therefore, the step is $t_{1nb} = 0.0122$ m.

Let us now present the main design relationships for shaping the nozzle blades and channels.

The nozzle blade chord is

$$b_{nb} = \frac{D_0 - D_{1nb}}{2\cos\alpha_{1e}}\,. \tag{21}$$

In calculations $b_{nb} = 19.3$ mm.

The nozzle blade width is

$$s_{nb} = a_{nb}\tan\alpha_{1e} + \Delta s\,, \tag{22}$$

where $\Delta s = \frac{1}{2}a_{nb} \cong 3.4$ mm. In calculations $s_{nb} = 8.8$ mm.

The diameter of the input edge of the nozzle blade can be presented as

$$d_{in} = c_{\max}, \tag{23}$$

where the maximum thickness of the blade profile is

$$c_{\max} = 2s_{nb}\tan\Delta\alpha + d_{out}. \tag{24}$$

In calculations $d_{in} = 3.2\,\text{mm}$.

The radius of curvature of the blade back is determined by the following equation

$$r_{nb} = (3-4)a_{nb}. \tag{25}$$

We select $r_{nb} = 20\,\text{mm}$.

Further, flow around the impeller in relative motion is considered. Since the working blades of the radial-axial turbine are straightforward, that is $\alpha_{1im} = 90\,\text{deg}$, the angle of attack (deg) is

$$i = 90 - \beta_1, \tag{26}$$

where β_1 is the angle of gas leakage in relative motion and is determined by the following relation

$$\beta_1 = \operatorname{arccot}\frac{c_1^{'}\cos\left(\alpha_{1e} - u_{1im}\right)}{c_1^{'}\sin\alpha_{1e}}, \tag{27}$$

where $c_1^{'} = c_1\dfrac{D_{1nb}}{D_{1im}}$.

In a cascade with a radial gas flow taking place in a radial-axial turbine, the following feature is revealed, namely, the angle α_{1e} is constant within the nozzle blade pitch. Note that the working blades, moving around the circle within a step, rotate in space by an angle of $\gamma = 18\,\text{deg}$, so the angles α_{1e} and β_1 will change. At the beginning of a step in motion $\alpha_{1e}^{'} = 38.4\,\text{deg}$, at the end of a step $\alpha_{1e}^{''} = \alpha_{1e}^{'} - \dfrac{\gamma}{2} = 29.4\,\text{deg}$. In this regard, the angle β_1 and the magnitude of velocity w_1 will change and this phenomenon, a change in the velocity w_1 with regard to the angle β_1 and magnitude, will occur unevenly at the point of passage of the edge of an adjacent nozzle blade; $\beta_1^{'} = 88.4\,\text{deg}$ is obtained for the angle $\alpha_{1e}^{'}$ and $\beta_1^{''} = 80.4\,\text{deg}$ is obtained for the angle $\alpha_{1e}^{''}$. Note that in our case the angles of attack *i* are always positive. The angles *i* in the flow around the blades are $i^{'} = +1.6\,\text{deg}$ and $i^{''} = +9.6\,\text{deg}$.

In addition to gas-dynamic edge tracks, additional disturbances arise, the frequency of which is

$$\nu = nz_{nb}. \tag{28}$$

In calculations $\nu = 28000\,\text{Hz}$.

In determining the angles of attack, a gas-dynamic calculation of the turbine was made with determining the relative velocity of the flow on the blades [13]:

$$w_1 = \sqrt{c_1^{'2} + u_{1im}^{\ 2} - 2c_1^{'}u_{1im}\cos\alpha_{1e}}. \tag{29}$$

In calculations, we obtain $w_1^{'} = 203\,\text{m/s}$ at $\alpha_{1e}^{'} = 38.4\,\text{deg}$ and $w_1^{''} = 182\,\text{m/s}$ at $\alpha_{1e}^{''} = 29.4\,\text{deg}$.

The impeller outlet gas velocity in the relative motion is

$$w_2 = \psi_{im}\sqrt{w_1^2 + 2L_{imS} - u_{1im}^{\ 2}\left(1 - \mu_{av}^{\ 2}\right)}, \tag{30}$$

where the velocity coefficient is $\psi_{im} = 0.85$, the available work of the impeller is $L_{imS} = L_{tS}\rho_t = 47.47$ kJ/kg. In calculations, we obtain $w_2' = 221.8$ m/s at $w_1' = 203$ m/s and $w_2'' = 208.2$ m/s at $w_1'' = 182$ m/s.

The MGTE thrust was determined by the total gas pressure behind the turbine P_t^* using the equation of the power balance of the compressor and turbine [13]:

$$P_t^* = P_{g0}^* \left[1 - \frac{k_g - 1}{k_g} \frac{G_a}{G_g} \frac{H_{cS}}{R_g T_{g0}^* \eta_c^* \eta_t^*} \right]^{\frac{k_g}{k_g - 1}}. \quad (31)$$

Here $k_g = 1.34$, $R_g = 287.5 \frac{\text{J}}{\text{kg} \cdot \text{K}}$, $G_a / G_g = 0.98$, $T_{g0}^* = 1100$ K, $\eta_c^* = 0.7$, $\eta_t^* = 0.76$ were taken. In calculations $P_t^* = 1.244 \times 10^5$ Pa.

According to the pressure drop, taking into account hydraulic losses in the nozzle and gas-dynamic functions, the outlet nozzle velocity is

$$c_n = \varphi_n \lambda_n \sqrt{\frac{2k_g}{k_g + 1} R_g T_t^*}, \quad (32)$$

where the nozzle velocity coefficient is $\varphi_n = 0.98$, the reduced speed is $\lambda_n = 0.59$, the gas temperature behind the turbine is $T_t^* = 840$ K. In calculations $c_n = 304$ m/s.

Then the MGTE thrust is

$$R = G_g c_n \sin \alpha_2. \quad (33)$$

Here the angle of gas exit from the turbine is $\alpha_2 = 83.8$ deg, mass flow gas through the nozzle is $G_g = 0.275$ kg/s. In the calculations, the thrust value was obtained $R = 82.7$ N.

COMBUSTOR DESIGN

A combustor was developed and manufactured for the MGTE created (Fig. 6). This combustor is made according to the reverse-flow scheme as shown in Fig. 7. The flame tube consists of the main part—the primary zone (PZ), the combustion zone (CZ), and the rotary (90 deg) outlet section—the mixing zone (MZ). After turning through 90 deg, the air from the compressor enters the intershaft duct and moves in the direction of the head, flowing into the flame tube through the three hole belts (P1, P2 and P3), then turns around the head, rotates by 180 deg and moves in the turbine direction flowing into the flame tube through two belt holes in its inner shell (P4 and P5). Let us present the distribution of the area of the holes in the air supply belts (in percent): $F_1 = 21.6$; $F_2 = 15.3$; $F_3 = 15.3$; $F_4 = 27.1$; $F_5 = 20.8$; $F_\Sigma = 100$.

Fig. 6.

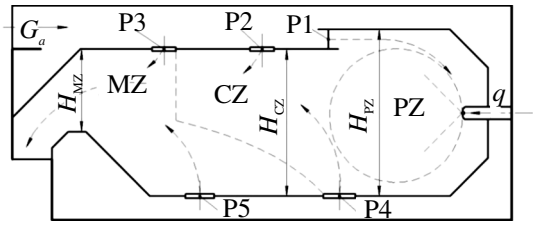

Fig. 7.

The outer diameter of the combustor is predetermined by the dimensions of the rotary part of the compressor diffuser, and the inner diameter of the combustor corresponds to the outer diameter of the wall of the output part of the turbine impeller. Taking into account the combustor inlet velocity $w_{comb}^{in} \le 40-60$ m/s, the dimensions of the external h_{isc}^{ext} and internal inter-sleeve channel h_{isc}^{int} are selected. The height of the flame tube in the primary zone H_{ft}^{PZ} is selected so that it has one toroidal vortex.

Then the primary zone length is

$$L^{PZ} = 1.1 H_{ft}^{PZ}; \tag{34}$$

the combustion zone length is

$$L^{CZ} = 2.5 H_{ft}^{av}, \tag{35}$$

where $H_{ft}^{av} = \dfrac{H_{ft}^{PZ} + H_{ft}^{CZ}}{2}$ is the average height of the flame tube in the combustion zone, and the length of the rotary section of the mixing zone is (Fig. 7):

$$L^{PZ} = 1 - 1.1 H_{ft}^{MZ}, \tag{36}$$

where H_{ft}^{MZ} is the height of the flame tube in the mixing zone.

For the selected dimensions, the structure of the flow and combustion in the combustor was calculated using the CFD ANSYS Fluent with the following boundary conditions: $P_c^* = 1.986 \times 10^5$ Pa, $T_c^* = 375$ K, $G_a = 0.275$ kg/s, $\alpha_{comb} = 3.3$.

Based on the calculation results it may be concluded that in the main part by air jets entering through the first belt of holes P1, a powerful vortex structure in the form of a toroidal vortex (Fig. 8) is formed in the outer shell of the flame tube (Fig. 7), providing efficient mixing of fuel with air and forming a combustible mixture with composition $\alpha_{PZ} \approx 0.5 \div 0.6$, at $T_g^* = 1500 \div 1600$ K (Fig. 9). Further, this mixture is diluted with secondary air (entering through the belt of holes in the inner ring P4), forming a mixture with composition $\alpha_{CZ} \approx 1 \div 1.5$, and burns out intensively at a temperature of $T_g^* = 1800 \div 2000$ K. After this, the combustion products are diluted by mixing them with air entering through the belts of the openings P5, P2 and the primary zone to a temperature of $T_g^* = 1100 \div 1200$ K. In this case, the temperature field at the inlet to the nozzle apparatus of the turbine has a uniform profile as in Fig. 9.

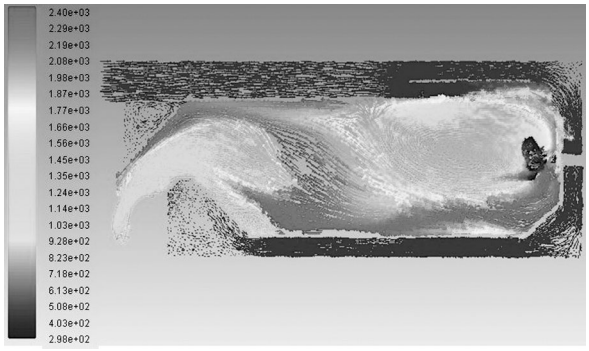

Fig. 8.

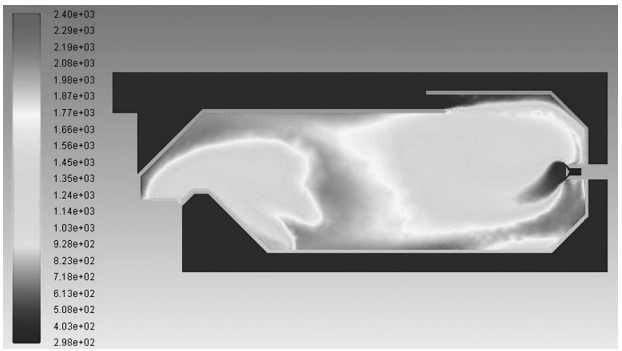

Fig. 9.

These calculations were performed without taking into account the cooling of the walls of the flame tube, which allowed us to reduce them in time by simplifying the computational grid and to determine the most heated regions of the walls of the flame tube, which should be supplied with cooling air during engine refinement tests.

Unlike large-size gas turbine engines, taking into account a need to reduce weight, there is no benefit in installing a separate lubrication system in a MGTE. In this case, the rotor bearings are lubricated with aviation kerosene from the engine fuel supply system (subsequently discarded into the jet nozzle). As a result, difficulties arise with the organization of bearings in the liquid friction mode, which leads to intensive wear of liners and shaft pins due to friction. It is also worth noting that the MGTE is characterized by significantly higher shaft speeds than those currently used in large-sized gas turbine engines.

CONCLUSIONS

Thus, in order to ensure an acceptable overhaul life and rotor speed during the creation of the MGTE, it became necessary to replace the bearings used in the turbocharger prototype. Currently, one of the most acceptable options that meet the requirements are full-metal-ceramic bearings, i.e. with ceramic rolling elements. Also note that in connection with the design changes of the turbocharger, it became necessary to reduce the initial shaft length.

As an output device, a subsonic jet nozzle with an extension pipe is used, the design of which is an extension tube ending with a fixed-geometry jet nozzle.

Analyzing the results of the work, we can conclude that the developed and manufactured MGTE can be used to create:

—a line of engines for flying models and special-purpose aircraft;

—a small-sized gas turbine power plant, using biogas or pure methane as a fuel, obtained from the processing of household waste;

—methodologies for the practical development of the MGTE, taking into account their design features and operating modes, including with the use of the ready-made assemblies of similar products.

REFERENCES

1. Judge, A.W., *Small Gas Turbines, and Free Piston Engines*, London: Chapman & Hall, 1960.
2. Natalevich, A.S., *Vozdushnye mikroturbiny* (Air Microturbines), Moscow: Mashinostroenie, 1979.
3. Schreckling, K., *Gas Turbine Engines for Model Aircraft*, London: Traplet Publications Ltd, 2003.
4. Kamps, T., *Model Jet Engines*, London: Traplet Publications Ltd, 2005.
5. Rostopchin, V.V., Micro-Turbojet Engine for Unmanned Aerial Vehicles, URL: http://www.uav.ru/articles/micro_trd.pdf.
6. Zhdanov, I.A., Staudacher, S., and Falaleev, S.V., Problems and Prospects of the Development of Microgas Turbine Engines for Unmanned Aerial Vehicles, *Vestnik Samarskogo Universiteta. Aerokosmicheskaya Tekhnika, Tekhnologii i Mashinostroenie*, 2011, no. 3–1 (27), pp. 345–353.
7. Kuz'michev, V.S., Tkachenko, A.Yu., and Ostapyuk, Ya.A., Features of Computer Simulation of the Working Process of Small-Sized Gas Turbine Engines, *Vestnik Samarskogo Universiteta. Aerokosmicheskaya Tekhnika, Tekhnologii i Mashinostroenie*, 2016, no. 4, pp. 91–101.
8. Kuz'michev, V.S., Tkachenko, A.Yu., and Filinov, E.P., The Influence of the Dimensions of a Gas Turbine Engine on the Choice of Optimal Parameters of the Workflow and Their Design Schemes, *Vestnik UGATU*, 2017, no. 1 (75), pp. 91–99.
9. Borovikov, D.A., Ionov, A.V., Seliverstov, S.D., and Yakovlev, A.A., Analysis of the Effect of the Additional Axial Stage of a Compressor on the Characteristics of Small-Sized Turbojet Engines, *Trudy MAI*, 2017, no. 96, URL: http://trudymai.ru/upload/iblock/33c/Borovikov_Ionov_Seliverstov_YAkovlev_rus.pdf?lang=ru&issue=96.

10. Large, J. and Pesyridis, A., Investigation of Micro Gas Turbine Systems for High Speed Long Loiter Tactical Unmanned Air Systems, *Aerospace*, 2019, vol. 6, no. 5. URL: https://www.mdpi.com/2226-4310/6/5/55/htm.
11. Capata, R. and Saracchini, M., Experimental Campaign Tests on Ultra Micro Gas Turbines, Fuel Supply Comparison and Optimization, *Energies*, 2018, vol. 11, no. 4, URL: https://www.mdpi.com/1996-1073/11/4/799/htm.
12. Mingazov, B.G., Limanskii, A.S., Sychenkov, V.A., Ankudimov, V,V., and S.S. Seyid Jafari, Small-Size Gas Turbine Engine for a Light Unmanned Aerial Vehicle, *Trudy Vserossiiskoi nauchno-prakticheskoi konferentsii "Aktual'nye problemy i perspektivy razvitiya grazhdanskoi aviatsii"* (Proc. of All-Russia Scientific and Practical Conference "Actual Problems and Prospects of the Civil Aviation Development"), Irkutsk: Irkutsk branch of MGTU GA, 2018, pp. 89–95.
13. Emin, O.N., Karasev, V.N., and Rzhavin, Yu.A., *Vybor parametrov i gazodinamicheskii raschet osevykh kompressorov i turbin aviatsionnykh GTD* (Selection of Parameters and Gas-Dynamic Calculation of Axial Compressors and Turbines for Aircraft GTEs), Moscow: Dipak, 2003.
14. Chistyakov, F.M., Ignatenko, V.V., Romanenko, N.T., N., and E.S. Frolov, *Tsentrobezhnye kompressornye mashiny* (Centrifugal Compressor Machines), Moscow: Mashinostroenie, 1969.
15. Baikov, B.P., Bordukov, V.G., Ivanov, P.V., and Deitch, R.S., *Turbokompressory dlya nadduva dizelei* (Turbochargers for Boosting Diesel Engines), Leningrad: Mashinostroenie, 1975.
16. Lokai, V.I., Maksutova, M.K., and Strunkin, V.A., *Gazovye turbiny dvigatelei letatel'nykh apparatov: Teoriya, konstruktsiya i raschet* (Gas Turbines of Aircarft Engines: Theory, Design and Calculation), Moscow: Mashinostroenie, 1991.
17. Sherstyuk, A.N. and Zaryankin, A.E., *Radial'no-osevye turbiny maloi moshchnosti* (Low Power Radial Axial Turbines), Moscow: Mashinostroenie, 1976.